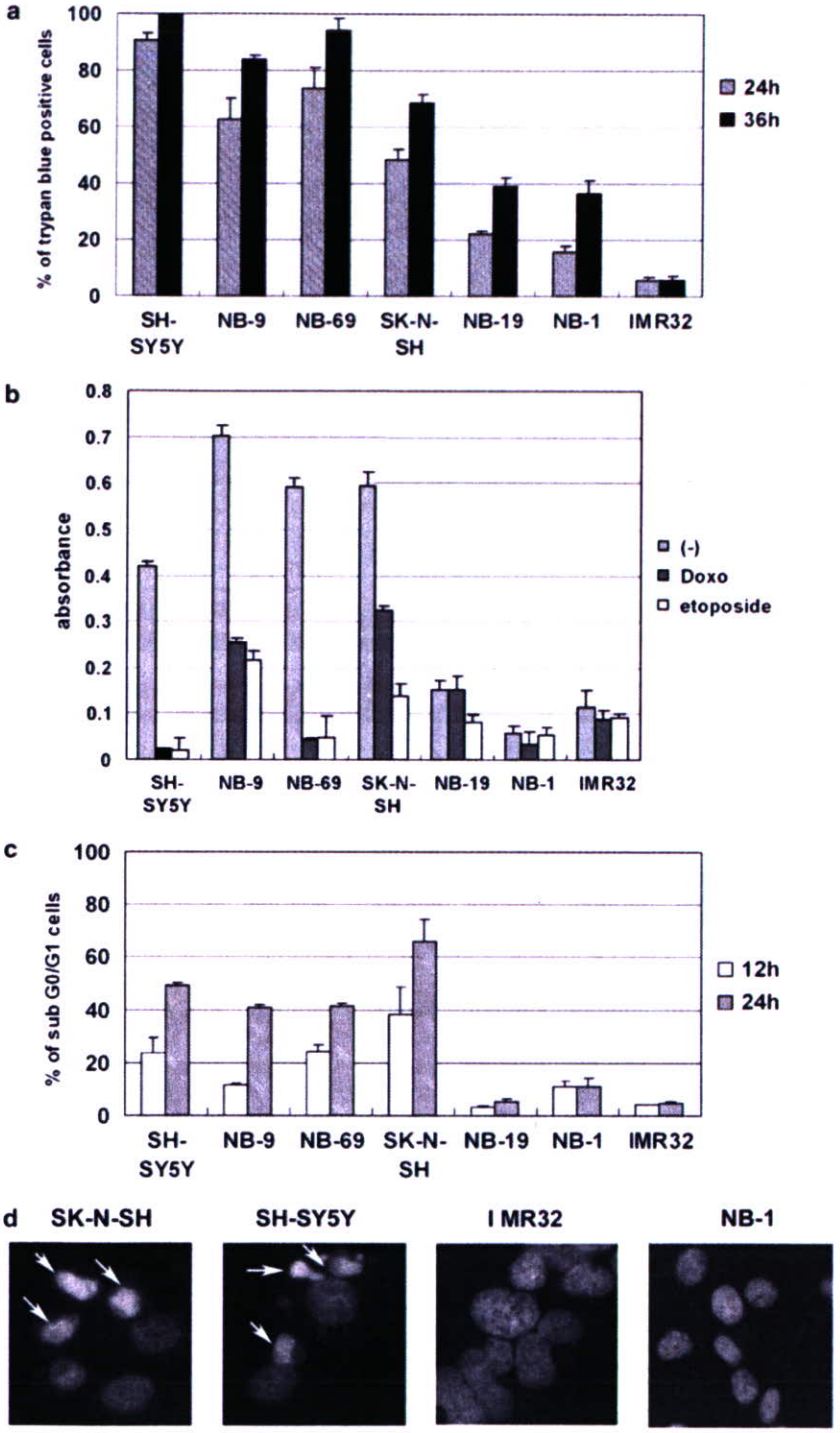

Figure 1 Sensitivity to doxorubicin (Doxo) is heterogenic in wild-type p53 harboring neuroblastoma (NB) cells. One hundred thousand cells were plated in a 3-cm-diameter culture dish and cultured in 5% CO_2 for 24 h. Doxo was added to the dish at 0.5 μg/ml and the incubation was continued for the indicated times. Mean and standard deviation (s.d.) of the % of cells were calculated for triplicate samples. (**a**) Cells were washed with 1 × phosphate-buffered saline (PBS), collected by 1 × PBS/0.5 mM EDTA, and stained with Trypan blue. The results are representative of four independent experiments. (**b**) After treatment of DNA-damaging reagents, cell viabilities were analysed by WST-8 assay. The results are representative of at least three independent experiments. (**c**) Analysis of the sub-G_0/G_1 fraction was performed as described in Materials and methods. The results are representative of three independent experiments. (**d**) Staining with 4′,6-diamidino-2-phenylindole (DAPI) was performed 24 h after Doxo stimulation. Arrows indicate the condensed or fragmented nuclei.

16G8 as an anti-phosphorylated p53ser15 antibody. Staining with pAb421 antibody revealed that the punctate cytoplasmic signal was upregulated in both Doxo-sensitive and -resistant NB cells after Doxo exposure (Figure 2c). DO1 antibody showed both nuclear and cytoplasmic staining before treatment, and remarkable accumulation into the nucleus was induced by Doxo in these four NB cell lines. Although ser15 phosphorylation was hardly

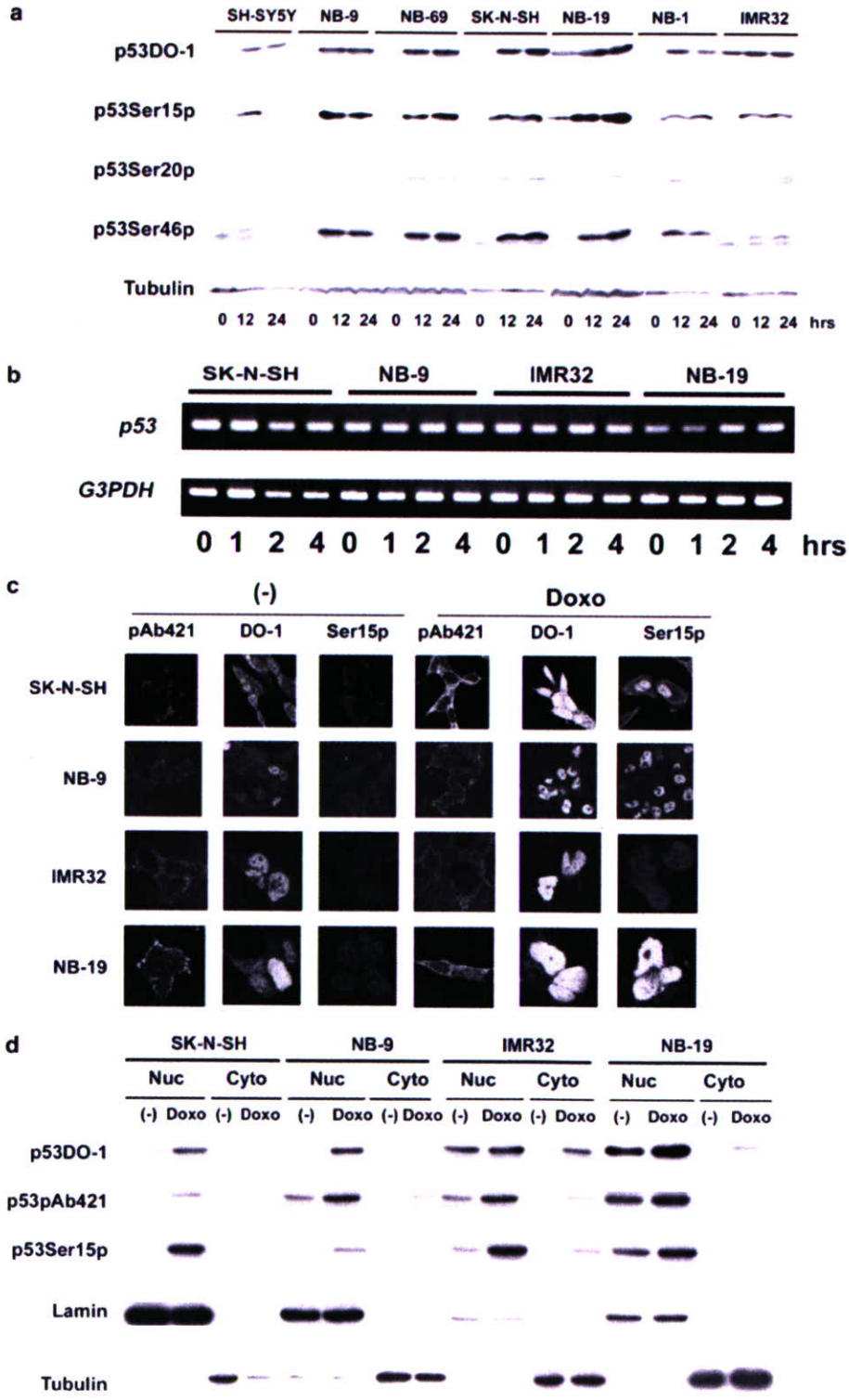

detected before treatment, the phosphorylation was remarkably upregulated by Doxo in SK-N-SH, NB-9 and NB-19 cells. In IMR32 cells, p53ser15 phosphorylation was modestly upregulated. The ser15-phosphorylated p53 accumulated to a much greater degree in the nucleus than in the cytoplasm after Doxo treatment. The use of several different fixation methods and modification of the first antibody concentration did not influence the results of immunofluorescence. Moreover, *p53* wild-type MCF7 cells showed similar staining results with these antibodies (data not shown). To investigate the observed discrepancy of p53 localization among the three monoclonal antibodies in the immunofluorescence experiments, we performed cell fractionation experiments (Figure 2d). All of the p53 signals were detected only in the nucleus before the treatment, and the upregulated signals induced by Doxo also accumulated in the nucleus rather than in the cytoplasm. The controls for fractionation, the nuclear marker lamin and cytoplasmic marker β-tubulin, were detected in the proper fractions and the amounts were not changed by Doxo treatment. These results show that the p53-dependent Doxo-stress increased the amount of p53 and induced the accumulation of p53 in the nucleus in both Doxo-sensitive and -resistant NB cells.

Activity of p53 as a transcriptional factor is required for Doxo-induced NB apoptosis

We then assessed the induction of p53-downstream molecules by Doxo. As shown in Figure 3a, exposure to Doxo induced remarkable $p21^{Cip1/Waf1}$ protein accumulation in the sensitive cells but not in the resistant cells, and this induction was caused at the transcriptional level (Figure 3b). HDM2 was similarly induced by Doxo treatment in the sensitive cells. However, *HDM2* mRNA accumulated in the resistant cells before Doxo treatment and did not change subsequently (Figure 3b), which is consistent with its protein accumulation (Figure 3a). These results indicate that the Doxo-induced cellular stress can effectively induce the p53 transcriptional activities in Doxo-sensitive NB cells but not in the resistant cells.

Doxo treatment induces synthesis of pro-apoptotic Noxa in the sensitive NB cells but not in the resistant cells

Next, we studied the expression of Bcl-2 family proteins in the NB cells, because regulation of the Bcl-2 family proteins by p53 is known to be the main component of p53-dependent apoptosis (Shen and White, 2001). The pro-apoptotic Bcl-2 family proteins Bax, Bak and Bok were not modified by Doxo in the NB cells (Figure 3a). Expression of Puma and p53AIP1 was also not affected by Doxo treatment (data not shown). It is interesting that Noxa was substantially induced only in the sensitive cells but not in the resistant cells. Although there was a considerable difference in the amount of anti-apoptotic Bcl-2 among the NB cells, its expression seemed not to be related to the Doxo sensitivity. The other anti-apoptotic Bcl-2 family protein Bcl-xL was not detected in any of the NB cells (data not shown). To assess whether the induction of Noxa is regulated at the transcriptional level, we performed semi-quantitative RT–PCR analysis. Consistent with the results of the western blot analysis, the mRNA amount of Noxa was clearly upregulated by Doxo treatment in the Doxo-sensitive SK-N-SH cells (Figure 3b). Meanwhile, the accumulation of *Noxa* mRNA expression was detected in the resistant cells (Figure 3b) and confirmed by quantitative real-time PCR analysis (Figure 3c). However, *Noxa* mRNA was not increased by Doxo treatment in the resistant cells (Figure 3b).

Noxa accumulation in mitochondria is not sufficient to induce apoptosis in NB cells

A recent report demonstrated that Noxa and Bok were induced by DNA stress dependent upon the p53 pathway in the SH-SY5Y cell line (Yakovlev *et al*., 2004). However, only Noxa upregulation was detected in the present study in the sensitive NB cell lines. Interestingly, larger amounts of Noxa were observed in the Doxo-resistant NB lines (IMR32 and NB-19) compared with the sensitive lines (SK-N-SH and NB-9). Since the organelle-specific amounts of the pro-apoptotic Bcl-2 family protein and its ratio to anti-apoptotic Bcl-2 family proteins in mitochondria are reported to determine cell fate in mitochondria-dependent apoptosis (Nakazawa *et al*., 2003; Danial and Korsmeyer, 2004), we studied the amounts of Noxa in mitochondria by cell fractionation/western blot analysis (Figure 4A). The amounts of Noxa in mitochondria were apparently upregulated in the sensitive cells. Densitometric analysis revealed that the Doxo-treatment increased the content of Noxa 10.3-fold in SK-N-SH cells and 16.6-fold in NB-9 cells compared to that before stimulation. On the other hand, Noxa was accumulated at higher levels in mitochondria of the resistant cells compared with the sensitive cells before Doxo treatment, and was not further increased by Doxo treatment. There were no significant differences in the amounts of Bcl-2 in the presence or absence of Doxo

Figure 2 Upregulation and nuclear accumulation of p53 in neuroblastoma (NB) cells. (**a**) Cells were collected after Doxo stimulation at the indicated time points (0, 12 and 24 h) and analysed by western blotting with the indicated antibodies (DO-1, p53ser15p, p53ser20p, p53ser46p and β-tubulin) as described in Materials and methods. (**b**) Cells were collected after Doxo stimulation at the indicated time points (0, 1, 2 and 4 h); p53 and G3PDH mRNA expression was analysed by RT–PCR as described in the Materials and methods section. (**c**) Cells were analysed by immunofluorescence with the indicated antibodies (pAb421, DO-1 and monoclonal anti-p53ser15p antibody: 16G8) 12 h after Doxo stimulation. (**d**) Cells were collected 12 h after Doxo stimulation and subjected to cell fractionation experiments as described in Materials and methods. Twenty micrograms of the proteins extracted from the organelle was analysed by sodium dodecyl sulfate–polyacrylamide gel electrophoresis (SDS–PAGE)/western blot experiments using the indicated antibodies. Lamin was used as a positive control for nuclear localization, and β-tubulin for cytosolic localization.

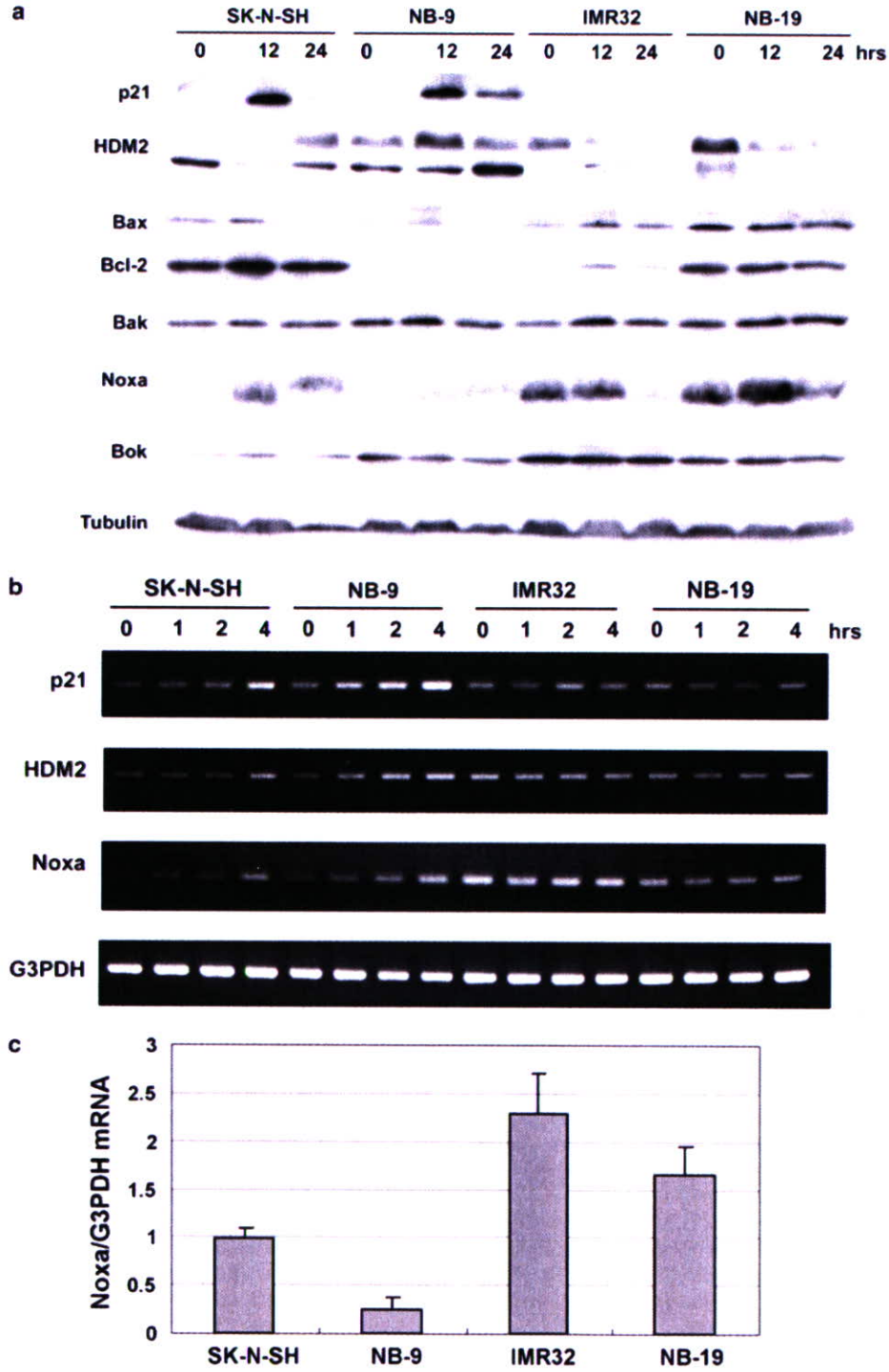

Figure 3 Modulation of p53-downstream proteins by Doxo treatment. The neuroblastoma (NB) cells were incubated with or without Doxo and collected at the indicated time points. **(a)** Extracted total cell lysates were subjected to sodium dodecyl sulfate–polyacrylamide gel electrophoresis (SDS–PAGE)/western blot analysis using the antibodies against the indicated molecules as described in Materials and methods. **(b)** Total RNA was subjected to semi-quantitative RT–PCR analysis as described in the Materials and methods section. **(c)** Quantitative real-time PCR analysis of *Noxa* mRNA amounts in NB cells as described in the methods section. Total RNA was extracted from unstimulated NB cells.

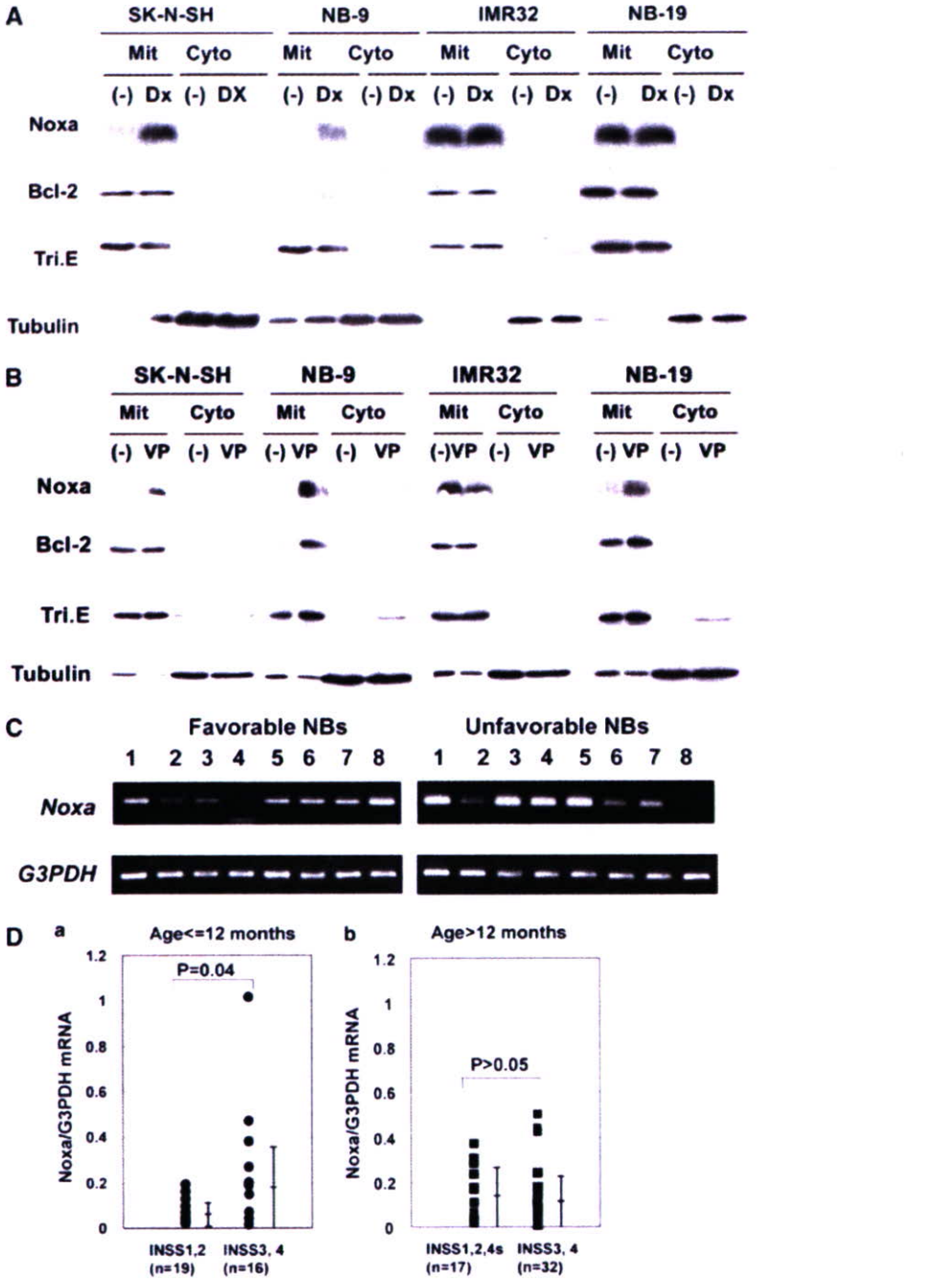

Figure 4 Noxa is upregulated in mitochondria by Doxo in the sensitive neuroblastoma (NB) cells. (**A** and **B**) Cells were collected 12 h after stimulation by Doxo (A, DX) or etoposide (B, VP) and subjected to cell fractionation for mitochondria (heavy membrane fraction: Mit) and the light membrane/cytosol fraction (Cyto). Samples were analysed by sodium dodecyl sulfate–polyacrylamide gel electrophoresis (SDS–PAGE)/western blotting with the indicated antibodies. Trifunctional protein (Tri E) and tubulin were controls for the mitochondrial fraction and cytosolic/light membrane fraction, respectively. This is a representative result of three independent experiments. (**C**) Semi-quantitative RT–PCR analysis of Noxa mRNA in favorable (stage 1 or 2, with single copy *MYCN*) and unfavorable (stage 3 or 4, with *MYCN* amplification) NB samples. (**D**) Quantitative real-time RT–PCR analysis of *Noxa* mRNA in 84 tumor samples from patients with NBs according to the tumor stage. The levels of Noxa were normalized to that of G3PDH. Results are presented as closed circles (**Da**) and closed squares (**Db**) with mean ± s.d. bars.

between the sensitive and resistant cells. Bcl-xL was not detected even by the fractionation experiments (not shown). The localization of trifunctional protein in mitochondria (Kamijo *et al*., 1993) and β-tubulin in the cytosol confirmed the reliability of the fractionation procedures. Importantly, similar results on the Noxa kinetics in mitochondria were observed after the treatment by etoposide, the other p53-dependent damage-inducing anticancer drug in NB cells (Figure 4B). Consistent with the results of WST-8 assay (Figure 1b), Noxa upregulation in mitochondria was observed in etoposide-sensitive SK-N-SH, NB-9 and NB-19 cells but not in IMR32 cells. These results suggest that the ratio of pro- to anti-apoptotic molecules such as Noxa/Bcl-2 has a strong impact on the p53-dependent damage-induced apoptosis in NB cells.

Next, we assessed *Noxa* mRNA amounts in NB tumor samples by semi-quantitative RT–PCR (Figure 4C) and quantitative real-time reverse transcriptional (RT)–PCR (Figure 4D). Consistent with the upregulation of *Noxa* mRNA in the resistant cell lines (Figures 3b and c), some unfavorable NB samples expressed large amounts of *Noxa* mRNA (Figure 4C). Especially, high levels of *Noxa* mRNA expression were significantly associated with INSS3 and INSS4 samples that were younger than 12 months old ($P = 0.04$) according to the Welch test (Figure 4D). In the NB samples that were older than 12 months old, no obvious difference was detected, mainly due to the high expression of Noxa in INSS 1 samples. Although we checked the correlation of *MYCN* and *Noxa* mRNA expression, there was no significant correlation (data not shown).

Knockdown of Noxa effectively reduces Doxo-induced cell death in NB cells

To definitively establish a role of Noxa in Doxo-induced cell death in NB cells, both of the sensitive SK-N-SH cells and the resistant IMR32 cells were treated with *Noxa* small interfering RNA (siRNA) and then the NB cells had Doxo administered. Preincubation of the NB cells with the *Noxa* siRNA but not control siRNA effectively reduced the *Noxa* mRNA and also protein amounts in SK-N-SH cells (Figures 5a and b). Since the effectiveness of *Noxa* siRNA1 is better than that of *Noxa* siRNA2, we used *Noxa* siRNA1 for later experiments. The *Noxa* siRNA1 did not affect the pro-apoptotic Bcl-2 family molecules (Bax and Bak), an important inhibitor of apoptosis $p21^{Cip1/Waf1}$ and interferon-α (Figure 5c), suggesting that the knockdown seems to have a specific effect on Noxa. The ability of the *Noxa* siRNA to reduce the *Noxa* mRNA amounts was accompanied by a significant reduction in the

Figure 5 Noxa knockdown cancels Doxo-induced apoptotic cell death in sensitive neuroblastoma (NB) cells. (**a**) SK-N-SH cells were collected 48 h after small interfering RNA (siRNA) treatment (lane 1: mock; lane 2: control siRNA; lane 3: Noxa siRNA1; lane 4: Noxa siRNA2) and subjected to cDNA synthesis/semi-quantitative RT–PCR procedure. (**b**) SK-N-SH cells (lane 3: mock; lane 4: control siRNA; lane 5: Noxa siRNA1; lane 6: Noxa siRNA2) were collected 48 h after siRNA treatment and 30 μg of proteins was subjected to sodium dodecyl sulfate–polyacrylamide gel electrophoresis (SDS–PAGE)/western blot analysis. Lanes 1 and 2 were nontreated IMR32 and NB-19 cells, respectively, as controls. (**c**) Forty-eight hours after the siRNA treatment, cells were treated with 0.5 μg/ml Doxo. Twenty-four hours after Doxo administration, SK-N-SH (lanes 1 and 2) and IMR32 (lanes 3 and 4) cells were collected and subjected to cDNA synthesis/semi-quantitative RT–PCR for the analysis of the molecules indicated at the left side of panel. Lanes 1 and 3 are control siRNA treated, and lanes 2 and 4 are Noxa siRNA1 treated. (**d** and **e**) Forty-eight hours after the siRNA treatment, cells were treated with 0.5 μg/ml Doxo. Twenty-four hours after Doxo administration, the culture dish-attached SK-N-SH and IMR32 cells were stained with 4′,6-diamidino-2-phenylindole (DAPI) and nuclear morphology was analysed. The floating cells were collected and subjected to Trypan blue uptake analysis. Trypan blue-positive cells were counted as 'dead cells.'

apoptotic morphological change of nuclei (nuclear condensation and fragmentation, Figure 5c) and cell death (Figure 5d) in the Doxo-sensitive SK-N-SH cells but not in the resistant IMR32 cells.

Doxo-induced stress induces mitochondrial dysfunction and activates the intrinsic caspase pathway

Next, we evaluated mitochondria homeostasis and activation of caspase pathways in NB cells. First, we investigated the role of mitochondrial membrane potential in Doxo-induced apoptosis. Mitochondrial membrane potential was assessed 10 h after Doxo stimulation by staining with the mitochondrion-selective dye, MitoTracker. Doxo-sensitive cells exhibited substantial mitochondrial depolarization, as evidenced by the loss of MitoTracker staining (Figure 6a). In contrast, depolarization was not induced by Doxo in the resistant cells. Next, immunofluorescence experiments showed that cytochrome-*c* was clearly released from mitochondria in the sensitive cells but not in the resistant cells (Figure 6b, Doxo-treated cells, 'Cyto. C' panels). Nuclear condensation was especially observed in the cells from which large amounts of cytochrome-*c* were released (Doxo-treated cells, 'Nuc' panels). These results suggest that mitochondrial dysfunction plays a pivotal role in Doxo-induced apoptosis in NB cells.

The central component of apoptosis is a proteolytic system involving a family of proteases called caspases (Green, 2000). As shown in Figure 6c, pro-caspase-9 cleavage was observed in the Doxo-sensitive cells, but not in the resistant cells 12 h after exposure to Doxo. The substrates of the activated caspase-9, pro-caspase-3 and -7 were also cleaved in the Doxo-sensitive cells. These findings suggest that apoptotic signals induced by Doxo activate the intrinsic caspase pathway via a mitochondrial pathway in NB cells, resulting in cell death of the Doxo-sensitive NB cells. Meanwhile, the resistant cells showed no activation of these initiator (caspase-9) and effector (caspase-3 and/or -7) caspases.

Discussion

Human *Noxa* is located on chromosome 18q21 and its promoter region contains a p53-responsive element (Oda *et al*., 2003). The expression of p53 increases human *Noxa* mRNA, and ectopic expression of Noxa effectively induces apoptosis in a BH3-motif-dependent manner (Oda *et al*., 2003). In the present study, we observed that Doxo-sensitive NB cells exhibited the Noxa mRNA/protein induction and protein localization into mitochondria after the treatment with Doxo, leading to an increase in the ratio of pro-/anti-apoptotic Bcl-2 family proteins. Mitochondrial dysfunction and intrinsic caspase-mediated apoptosis were also induced in the sensitive cells. Notably, apoptosis was almost completely canceled by the knockdown of Noxa by siRNA, confirming the importance of Noxa in the Doxo-induced apoptosis of NB cells. Taken together, these findings indicate that the Noxa upregulation in mitochondria may play an important role in Doxo-induced apoptosis in NB cells. A previous study described that Noxa and Bok were induced by etoposide, and *Noxa* siRNA treatment reduced etoposide-induced cell death in SH-SY5Y NB cells (Yakovlev *et al*., 2004). Furthermore, Obexer *et al*. (2007) reported that Noxa and Bim are effectors of FKHRL-1-induced apoptosis in NB cells. Since we also observed the upregulation of Noxa in mitochondria by Doxo or etoposide treatment, Noxa seems to be one of the important effectors of the pro-apoptotic signaling pathway in NB cell apoptosis.

Whereas Yakovlev *et al*. (2004) did not use stress-resistant NB cells, the kinetics of Noxa induction in the stress-resistant NB cells was evaluated in our study. In the Doxo-resistant NB cells, exposure to Doxo failed to increase the expression of Noxa and the other downstream molecules in mitochondria, although p53 was abundant in the nucleus before Doxo exposure and some of the p53 serine residues that regulate p53 stability and activity (Shieh *et al*., 1997; Oda *et al*., 2000) were efficiently phosphorylated in the resistant cells, as well as in the sensitive cells. These results suggest that the lack of some p53 function in the resistant NB cells results in the failure of apoptosis, even under the pressure of DNA damage, such as Doxo treatment. It is of interest that the amounts of *Noxa* mRNA and protein in the mitochondria were much larger in the unstimulated resistant cells than in the sensitive cells but not stimulated by Doxo treatment. Alternatively, the inability to upregulate Noxa transcription in response to Doxo may be related to resistance to the anthracycline in some NB cells. Large amounts of *Noxa* mRNA in a part of unfavorable NB primary tumor samples (Figure 4C) supported the observation of inactivity of accumulated Noxa in the resistant cells. The accumulation of Noxa in unstimulated NB cells seems to be p53 independent, as it was suggested by our experiments. Although several findings suggest that Noxa is induced via a p53-independent pathway in neuronal cells (Kiryu-Seo *et al*., 2005; Wong *et al*., 2005), the exact molecular pathway responsible for the p53-independent Noxa induction in NB remains to be elucidated. One possibility is the presence of other p53 family proteins, for example, p63 and p73 proteins in NB cells. Actually, p73-alpha is expressed in several NB cell lines, including IMR32 and NB19 cells, and p63, but not deltaNp63, is highly expressed at the transcriptional level in IMR32 cells (data not shown). The study of the physiological role of p63 and p73 proteins on Noxa expression and Doxo-induced NB cell death seems to be meaningful for research of NB cell death.

A previous report indicated that although Noxa expression mediated by adenovirus could not induce apoptosis in either wild-type or *p53*-knockout MEFs, its expression effectively enhanced the apoptotic response to etoposide or UV (Shibue *et al*., 2003), suggesting that Noxa induces apoptosis in concert with not only p53-dependent cellular signals, but also p53-independent cellular signals. Additionally, we found a significant increase of *Noxa* mRNA amounts in the tumor samples

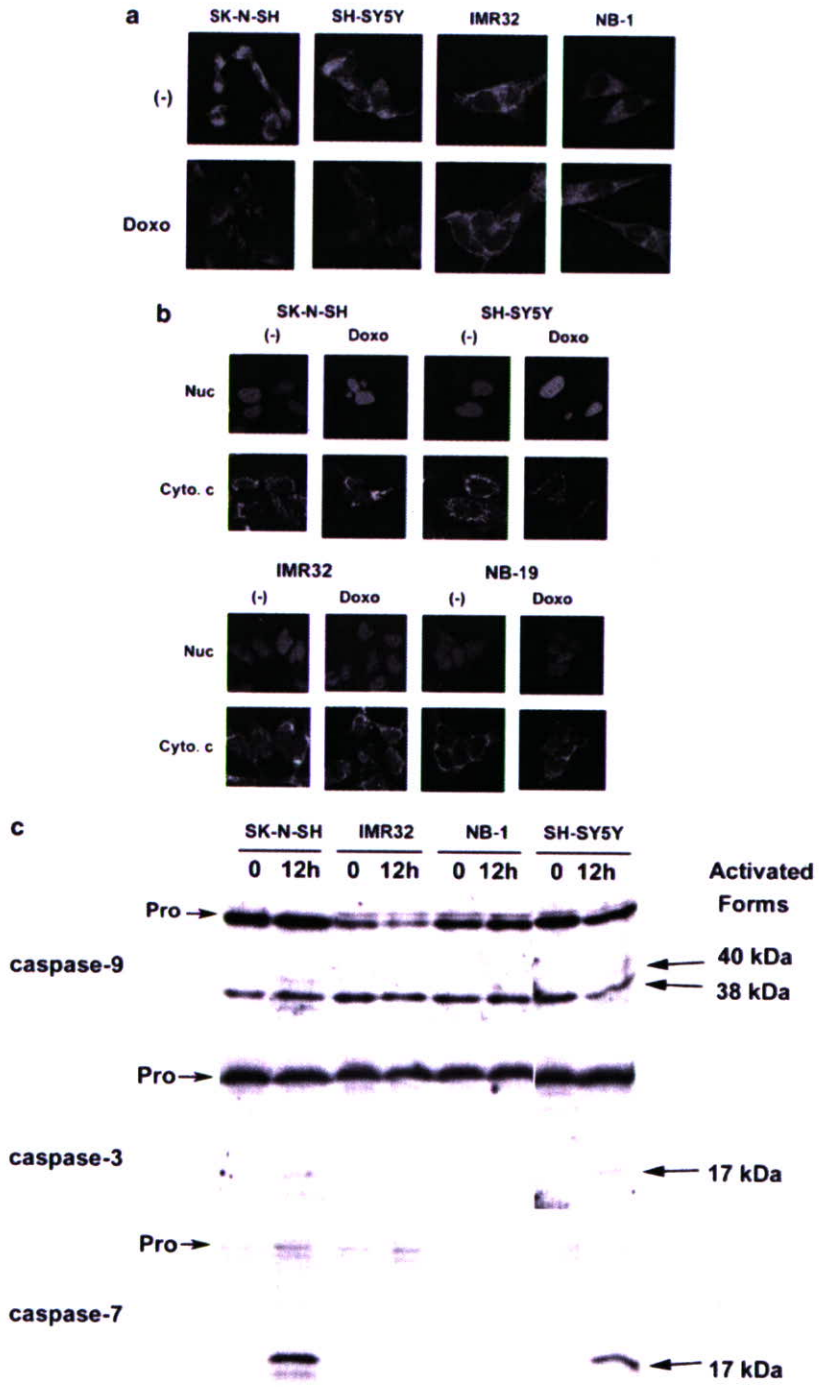

Figure 6 Mitochondrial dysfunction is induced by Doxo in the sensitive neuroblastoma (NB) cells. (**a**) Mitochondrial membrane potential was detected using MitoTracker dye 6 h after Doxo stimulation (Doxo). The steady-state potential is shown as a control [(−)]. (**b**) Cells were stimulated with Doxo for 6 h, and then cytochrome-*c* (Cyto. c) signals were detected by immunofluorescence experiments. The nucleus (Nuc) was stained with 4′,6-diamidino-2-phenylindole (DAPI). (**c**) Cells were collected at the indicated time points after Doxo stimulation and subjected to sodium dodecyl sulfate–polyacrylamide gel electrophoresis (SDS PAGE)/western blot analysis. Processing of pro-caspase-9 was detected by the presence of 38/40-kDa cleaved forms. The anti-caspase-3 rabbit polyclonal antibody (BD Pharmingen) recognized the 32-kDa pro-caspase-3 and the 17-kDa cleaved form. The anti-caspase-7 mouse monoclonal antibody (clone B94-1) recognized the 35-kDa pro-caspase-7 and the 17-kDa cleaved form.

in the advanced stage (INSS3 and -4, younger than 12 months old) by quantitative real-time RT–PCR analysis (Figure 4D), indicating that the inactiveness of *Noxa* may relate to the progression in NB tumors. These observations suggest that reactivation of the accumulated Noxa in the Doxo-resistant NB cells with p53-independent stress may provide a new therapeutic approach to chemotherapy-resistant NB. Moreover, biochemical analysis of the accumulated Noxa in the mitochondria of resistant cells, for example, the analysis of Noxa-binding Bcl-2-family proteins in mitochondria, may be useful to address the mechanism of the failure of Doxo-induced apoptosis in those cells.

To address the other potential mechanisms of the resistances of DNA-damage-induced reagents in the chosen cell lines, we studied the genomic amplification of *MYCN* (Materials and methods), *caspase-8* and *P-glycoprotein* mRNA expression by semi-quantitative RT–PCR (data not shown). Caspase-8 was expressed in NB-9, NB-69, SK-N-SH and NB-1 cells. However, caspase-8 seems not to have a significant role in the Doxo-induced NB apoptosis, since we could not detect its activation by western blotting (data not shown). P-glycoprotein was clearly expressed in NB-9, NB-69, SK-N-SH and NB-1 cells, but not in SH-SY5Y, NB-1, and IMR32 cells (data not shown), suggesting that p-glycoprotein seems not to relate to the Doxo sensitivity of NB cells. Regarding *MYCN* amplification status, all the three resistant cell lines had *MYCN* amplification and three of four sensitive cell lines had single copy *MYCN*, suggesting that inactivity of p53 in the resistant cell lines may relate to the *MYCN* amplification. Consistent with our observation, Bell *et al.* (2006) reported that *MYCN* amplification correlates with attenuated $p21^{Cip1/Waf1}$ induction in *p53* wild-type NB cells. The analysis of the molecular mechanism between *MYCN* amplification and p53 inactivation in NB cells may be important for NB studies.

Taken together, our findings indicate that the p53 pathway regulates NB cell apoptosis via pro-apoptotic Noxa kinetics and localization in the mitochondria. Further study of Noxa in NB may provide an important approach to develop new therapies for NB and to improve the prognosis of high-risk NB patients.

Materials and methods

Reagents and antibodies

Anti-p53 mouse monoclonal antibody (clone DO-1), anti-Bcl-2 mouse monoclonal antibody (clone C-2), anti-$p21^{Cip1/Waf1}$ mouse monoclonal antibody (clone F-5) and anti-Bad mouse monoclonal antibody (clone C-7) were from Santa Cruz Biotechnology Inc. (Santa Cruz, CA, USA). Anti-cytochrome-*c* mouse monoclonal antibody (clone 7H8.2C12), anti-Bcl-xL mouse monoclonal antibody (clone 2H12), anti-caspase-3 rabbit polyclonal antibody, anti-caspase-7 mouse monoclonal antibody (clone B94-1) and anti-Bid rabbit polyclonal antibody were from BD PharMingen (San Diego, CA, USA). Anti-phospho-p53 rabbit serum (p53ser15p, p53ser20p and p53ser46p) and anti-phospho-p53ser15 mouse monoclonal antibody (clone 16G8) were from Cell Signaling Technology (Beverly, MA, USA). Anti-Bax and Anti-Bak rabbit polyclonal antibodies were from Upstate Biotechnology (Lake Placid, NY, USA). Anti-p53 mouse monoclonal antibody (clone pAb421), anti-p53 sheep polyclonal Antisera (Ab-7) Kit and anti-Noxa mouse monoclonal antibody (clone 114C307, for immunofluorescence analysis) were from Oncogene Research Products (Cambridge, MA, USA). Anti-Noxa rabbit polyclonal antibody (for western blotting) was from Abcam (Cambridge, UK). Anti-Bim rabbit polyclonal antibody was from Millennium Biotechnology (Ramona, CA, USA). Anti-Bok rabbit polyclonal antibody was from ABGENT (San Diego, CA, USA). Anti-caspase-9 mouse monoclonal antibody (clone 5B4) was from MBL (Nagoya, Japan). Anti-lamin monoclonal antibody (clone JOL2) was from Chemicon (Temecula, CA, USA). Anti-β-tubulin mouse monoclonal antibody (clone KMX-1) was from Roche Diagnostics (Manheim, Germany). Anti-trifunctional protein serum was prepared by rabbit immunization and affinity selection with purified trifunctional protein (Kamijo *et al.*, 1993). Anti-HDM2 monoclonal antibody (clone 2A10) was a generous gift from Dr Arnold J Levine, Pediatrics and Biochemistry Cancer Institute of New Jersey. Other biochemical reagents were purchased from Sigma-Aldrich Japan, or Wako (Osaka, Japan).

Cells and cell culture

We collected p53 wild-type NB cell lines to study the role of the p53 pathway in drug resistance mechanism of NB cells. SK-N-SH, NB-9, NB-19 and NB69 were obtained from Riken Cell Bank (Tsukuba, Japan). IMR32 and NB-1 were from Cell Resource Center for Biomedical Research Institute of Development, Aging and Cancer, Tohoku University. The wild-type *p53*-expressing SH-SY5Y line was purchased from ATCC (Manassas, VA, USA). The wild-type p53 status was demonstrated in previous reports (IMR32: Hopkins-Donaldson *et al.*, 2002; SK-N-SH: Wolff *et al.*, 2001) and p53 sequencing, which was performed according to the previous report (Tweddle *et al.*, 2001), confirmed the wild-type p53 status in these cell lines. In terms of the copy number of MYCN by Southern blot analysis, SH-SY5Y, SK-N-SH and NB-69 are single-copy NB cells; NB-9, IMR32, NB-1 and NB-19 cells have 50, >150, >150 and 25 copies, respectively (data not shown). The cells were routinely maintained with DMEM supplemented with 10% fetal bovine serum (FBS) and 1 × penicillin/streptomycin (Invitrogen, Carlsbad, CA, USA).

Tumor samples

Fresh, frozen tumor tissues were sent to the Division of Biochemistry, Chiba Cancer Center Research Institute, from various hospitals in Japan with informed consent from the patients' parents. All samples were obtained by surgery or biopsy and stored at −80°C. More than 70% of tumor cell contents of the samples were confirmed by pathological analysis of the adjacent tissues. Studies were approved by the Institutional Review Board of the Chiba Cancer Center.

Cell proliferation assay

NB cells were seeded in 96-well plates at a density of 10^4 cells/well in a final volume of 100 μl. Twenty-four hours after seeding, the medium was removed and replaced with fresh medium or with medium containing 0.5 μg/ml of Doxo or 20 μM etoposide in a final volume of 100 μl. The culture was maintained in the 5% CO_2 for 24 h and then 10 μl of WST-8 labeling solution (Cell Counting Kit-8, DOJINDO, Kumamoto, Japan) was added, and the cells were returned to the incubator for 4 h. The absorbance of the formazan product formed was

Table 1 Sequence of primers for PCR experiments

Gene	*Forward primer sequence*	*Reverse primer sequence*	*Accession number*
p53	cagccaagtctgtgacttgcacgtac	ctatgtcgaaaagtgtttctgtcatc	NM_000546
$p21^{Cip1/Waf1}$	gacaccactggagggtgact	ggcgtttggagtggtagaaa	L25610
HDM2	tagtagcattatttatagcagcc	agagaagaaatctatgtgaattgag	Z12020
Noxa	agagctggaagtcgagtgt	gcaccttcacattcctctc	D90070
Bax	ttttgcttcagggtttcatc	cagttgaagttgccgtcaga	BC014175
Bak1	gccttttgcagttggactctc	gggttgggagcaagtgtcta	NM_001188
IFN-α1	caatatctacgatggcctcgc	agagatggctggagccttctg	NM_024013
Caspase-8	gggacaggaatggaacacac	gccatagatgatgccccttgt	AF009620
P-glycoprotein	gaatctggaggaagacatgacc	tccaattttgtcaccaattcc	NM_000927
G3PDH	accacagtccatgccatcac	tccaccaccctgttgctgta	NM_002046

detected at 450 nm in a 96-well spectrophotometric plate reader, as per the manufacturer's protocol.

Morphological analysis of apoptosis and analysis of sub-G_0/G_1 fraction

Cells were observed using a phase-contrast microscope to assess apoptotic morphological changes and treated with 4′,6-diamidino-2-phenylindole (DAPI), a DNA-staining dye, to detect the morphological characteristics of apoptotic nuclei, namely, condensation and fragmentation, after fixation with 3.7% (v/v) formaldehyde/1 × phosphate-buffered saline (PBS). Analysis of sub-G_0/G_1 fraction was performed by using the method described in the previous report (Nakazawa *et al*., 2003).

Immunofluorescence

Fixation was performed with 3.7% (v/v) formaldehyde/1 × PBS for 30 min and the permeabilization was done with 0.1% (v/v) TritonX-100/1 × PBS for 5 min at room temperature. Cells were then stained for 1 h with the first antibody followed by a 30-min exposure to an appropriate second antibody conjugated with fluorescent dye (Alexa488 or Alexa594). DNA was visualized with DAPI or propidium iodide. Analysis by confocal laser microscopy was performed with an LSM510 system (Carl Zeiss, Oberkochen, Germany).

Cell fractionation and direct western blotting

For the isolation of the heavy membrane faction (Mito) in Figures 4A and B, 2×10^6 cells were subjected to the fractionation procedure described previously (Nakazawa *et al*., 2003). The resulting supernatant after isolation of Mito was referred to as the cytosol plus light membrane (Cyto) fractions.

For isolation of the nucleus (Nuc) in Figure 2d, 1×10^6 cells were suspended in 0.4 ml of buffer (10 mM HEPES pH 7.9, 10 mM KCl, 1.5 mM $MgCl_2$, 0.5 mM DTT, 0.4 μM PMSF), and incubated on ice for 20 min. After vortexing for 1 min at the maximum setting, cells were centrifuged at 15 000 r.p.m. for 10 s, and then the supernatant was kept as cytosol (Cyto). The pellet was resuspended in 0.1 ml of buffer (20 mM HEPES pH 7.9, 420 mM NaCl, 1.5 mM $MgCl_2$, 0.2 mM EDTA, 25% (v/v) glycerol, 0.5 mM DTT, 0.4 μM PMSF), and incubated on ice for 20 min. Then the cells were centrifuged at 15 000 r.p.m. for 2 min, and then the supernatant was kept as nucleus (Nuc). Direct western blotting was performed according to the previous report (Nakazawa *et al*., 2003).

Preparation of mRNA and analysis of RNA expression

Total RNA was extracted from NB cells using Isogen (Wako, Tokyo, Japan), and cDNA was synthesized from 1 μg of total RNA templates according to the manufacturer's protocol (RiverTra-Ace-α- RT–PCR kit, TOYOBO, Osaka, Japan). PCR amplification of either p53 or Noxa was performed using previously reported primers (for p53: Paull and Whitehart, 2005; for Noxa: Ohtani *et al*., 2004). The other primer sequences are listed in Table 1. RT-PCR products (~0.5 kb) were detected by direct ethidium bromide staining after electrophoretic separation on agarose gels. RT-PCR analysis of G3PDH mRNA expression was performed as a positive control for these experiments according to the manufacturer's protocol (RiverTra-Ace -α- RT–PCR kit). Semi-quantitative RT-PCR analysis of tumor samples was performed according to the previous report (Machida *et al*., 2006). The PCR amplification was performed using the above-mentioned primers for Noxa.

Quantitative real-time PCR analysis

For quantification of Noxa in primary NB samples, cDNA was synthesized with random primers Superscript II reverse transcriptase (GibcoBRL) from 15 μg of primary tumor total RNA. Noxa and GAPDH primers and probes were purchased from Applied Biosystems (Noxa Assay ID: Hs00560402_m1; GAPDH: Pre-Developed TaqMan Assay Reagents Human G3PDH). Quantitative real-time PCR analysis was performed by ABI7700 Prism sequence detector (Applied Biosystems, Foster City, CA, USA), according to the manufacturer's instructions using 1 × TaqMan Universal PCR Master Mix. After denaturing at 95°C for 10 min, PCR amplification was performed by 50 cycles of denaturation at 95°C for 15 s and annealing/extension at 60°C for 1 min. A quantification of *Noxa* mRNA in each sample was performed by comparing with the standard curve, which was generated by reacting the plasmid containing human Noxa (Hijikata *et al*., 1990). Furthermore, G3PDH mRNA quantification was also performed for a standardization of the initial RNA content of each sample.

Small interference RNA transfection

Noxa small interference RNAs were synthesized according to the previous experiments (Noxa siRNA1, Qin *et al*., 2004: 5′-TCAGTCTACTGATTTACTGG-3′; Noxa siRNA2, Lee *et al*., 2005: 5′-AACTTCCGGCAGAAACTTCTG-3′). Control siRNA (Silencer Negative Control #1 siRNA) was purchased from Ambion Inc. (Austin, TX, USA). NB cells were plated at a density of 3×10^5 cells in a 3-cm-diameter dish. Small interference RNA duplexes (10 nM) were transfected with Lipofectamine™ RNAiMAX in Opti-MEM medium according to the manufacturer's protocol. After 24 h, transfected cells were treated with Doxo for another 24 h.

Statistical analysis

The Welch test was used as a statistical method of parametric test to explore possible associations between Noxa expression and other factors, using StatView ver. 4.11 (Abacus Concepts

Inc., Cheltenham, UK). Statistical significance was declared if the *P*-value was <0.05.

Acknowledgements

We are deeply indebted to Professor Kenichi Koike (Department of Pediatrics, Shinshu University School of Medicine) for his excellent advice. We thank Kumiko Sakurai, Yozo Nakazawa, and Jun Miki for their technical assistance, and Daniel Mrozek, Medical English Service Inc, for editorial assistance. This work was supported by grants from the Japanese Ministry of Education, Science, Sports and Culture, Grant-in-Aid for Scientific Research (C) (contract nos: 15591098 and 17591077).

References

Aleyasin H, Cregan SP, Iyirhiaro G, O'Hare MJ, Callaghan SM, Slack RS *et al.* (2004). Nuclear factor-(kappa)B modulates the p53 response in neurons exposed to DNA damage. *J Neurosci* **24**: 2963–2973.

Bell E, Premkumar R, Carr J, Lu X, Lovat PE, Kees UR *et al.* (2006). The role of MYCN in the failure of MYCN amplified neuroblastoma cell lines to G1 arrest after DNA damage. *Cell Cycle* **5**: 2639–2647.

Danial NN, Korsmeyer SJ. (2004). Cell death: critical control points. *Cell* **116**: 205–219.

Green DR. (2000). Apoptotic pathways: paper wraps stone blunts scissors. *Cell* **102**: 1–4.

Hempel G, Flege S, Wurthwein G, Boos J. (2002). Peak plasma concentrations of doxorubicin in children with acute lymphoblastic leukemia or non-Hodgkin lymphoma. *Cancer Chemother Pharmacol* **49**: 133–141.

Hijikata M, Kato N, Sato T, Kagami Y, Shimotohno K. (1990). Molecular cloning and characterization of a cDNA for a novel phorbol-12-myristate-13-acetate-responsive gene that is highly expressed in an adult T-cell leukemia cell line. *J Virol* **64**: 4632–4639.

Hopkins-Donaldson S, Yan P, Bourloud KB, Muhlethaler A, Bodmer JL, Gross N. (2002). Doxorubicin-induced death in neuroblastoma does not involve death receptors in S-type cells and is caspase-independent in N-type cells. *Oncogene* **21**: 6132–6137.

Hudson CD, Morris PJ, Latchman DS, Budhram-Mahadeo VS. (2005). Brn-3a transcription factor blocks p53-mediated activation of proapoptotic target genes Noxa and Bax *in vitro* and *in vivo* to determine cell fate. *J Biol Chem* **280**: 11851 11948.

Isaacs JS, Saito S, Neckers LM. (2001). Requirement for HDM2 activity in the rapid degradation of p53 in neuroblastoma. *J Biol Chem* **276**: 18497–18506.

Kamijo T, Aoyama T, Miyazaki J, Hashimoto T. (1993). Molecular cloning of the cDNAs for the subunits of rat mitochondrial fatty acid beta-oxidation multienzyme complex. Structural and functional relationships to other mitochondrial and peroxisomal beta-oxidation enzymes. *J Biol Chem* **268**: 26452–26460.

Keshelava N, Zuo JJ, Chen P, Waidyaratne SN, Luna MC, Gomer CJ *et al.* (2001). Loss of p53 function confers high-level multidrug resistance in neuroblastoma cell lines. *Cancer Res* **61**: 6185–6193.

Kiryu-Seo S, Hirayama T, Kato R, Kiyama H. (2005). Noxa is a critical mediator of p53-dependent motor neuron death after nerve injury in adult mouse. *J Neurosci* **25**: 1442–1447.

Komarova EA, Chernov MV, Franks R, Wang K, Armin G, Zelnick CR *et al.* (1997). Transgenic mice with p53-responsive lacZ: p53 activity varies dramatically during normal development and determines radiation and drug sensitivity *in vivo*. *EMBO J* **16**: 1391–1400.

Letai A, Bassik MC, Walensky LD, Sorcinelli MD, Weiler S, Korsmeyer SJ. (2002). Distinct BH3 domains either sensitize or activate mitochondrial apoptosis, serving as prototype cancer therapeutics. *Cancer Cell* **2**: 183–192.

Lee SJ, Kim KM, Namkoong S, Kim CK, Kang YC, Lee H *et al.* (2005). Nitric oxide inhibition of homocysteine-induced human endothelial cell apoptosis by down-regulation of p53-dependent Noxa expression through the formation of S-nitrosohomocysteine. *J Biol Chem* **280**: 5781–5788.

Lowe SW, Bodis S, McClatchey A, Remington L, Ruley HE, Fisher DE *et al.* (1994). p53 status and the efficacy of cancer therapy *in vivo*. *Science* **266**: 807–810.

Machida T, Fujita T, Ooo ML, Ohira M, Isogai E, Mihara M *et al.* (2006). Increased expression of proapoptotic BMCC1, a novel gene with the BNIP2 and Cdc42GAP homology (BCH) domain, is associated with favorable prognosis in human neuroblastomas. *Oncogene* **25**: 1931–1942.

Matthay KK, Perez C, Seeger RC, Brodeur GM, Shimada H, Atkinson JB *et al.* (1998). Successful treatment of stage III neuroblastoma based on prospective biologic staging: a Children's Cancer Group study. *J Clin Oncol* **16**: 1256–1264.

Moll UM, LaQuaglia M, Bénard J, Riou G. (1995). Wild-type p53 protein undergoes cytoplasmic sequestration in undifferentiated neuroblastomas but not in differentiated tumors. *Proc Natl Acad Sci USA* **92**: 4407–4411.

Moll UM, Ostermeyer AG, Haladay R, Winkfield B, Frazier M, Zambetti G. (1996). Cytoplasmic sequestration of wild-type p53 protein impairs the G1 checkpoint after DNA damage. *Mol Cell Biol* **16**: 1126–1137.

Nakazawa Y, Kamijo T, Koike K, Noda T. (2003). ARF tumor suppressor induces mitochondria-dependent apoptosis by modulation of mitochondrial Bcl-2 family proteins. *J Biol Chem* **278**: 27888–27895.

Obexer P, Geiger K, Ambros PF, Meister B, Ausserlechner MJ. (2007). FKHRL1-mediated expression of Noxa and Bim induces apoptosis via the mitochondria in neuroblastoma cells. *Cell Death Diff* **14**: 534–547.

Oda E, Ohki R, Murasawa H, Nemoto J, Shibue T, Yamashita T *et al.* (2003). Noxa, a BH3-only member of the Bcl-2 family and candidate mediator of p53-induced apoptosis. *Science* **17**: 1053–1058.

Oda K, Arakawa H, Tanaka T, Matsuda K, Tanikawa C, Mori T *et al.* (2000). p53AIP1, a potential mediator of p53-dependent apoptosis, and its regulation by Ser-46-phosphorylated p53. *Cell* **102**: 849–862.

Ohtani S, Kagawa S, Tango Y, Umeoka T, Tokunaga N, Tsunemitsu Y *et al.* (2004). Quantitative analysis of p53-targeted gene expression and visualization of p53 transcriptional activity following intratumoral administration of adenoviral p53 *in vivo*. *Mol Cancer Ther* **3**: 93–100.

Oren M. (1999). Regulation of the p53 tumor suppressor protein. *J Biol Chem* **274**: 36031–36034.

Paull AC, Whikehart DR. (2005). Regulation of the p53 tumor suppressor protein. *Mol Vis* **11**: 328–334.

Qin JZ, Stennett L, Bacon P, Bodner B, Hendrix MJ, Seftor RE *et al.* (2004). p53-independent NOXA induction overcomes apoptotic resistance of malignant melanomas. *Mol Cancer Ther* **3**: 895–902.

Shen Y, White E. (2001). p53-dependent apoptosis pathways. *Adv Cancer Res* **82**: 55–84.

Shibue T, Takeda K, Oda E, Tanaka H, Murasawa H, Takaoka A *et al.* (2003). Integral role of Noxa in p53-mediated apoptotic response. *Genes Dev* **17**: 2233–2238.

Shieh SY, Ikeda M, Taya Y, Prives C. (1997). DNA damage-induced phosphorylation of p53 alleviates inhibition by MDM2. *Cell* **91**: 325–334.

Tweddle DA, Malcolm AJ, Bown N, Pearson AD, Lunec J. (2001). Evidence for the development of p53 mutations after cytotoxic therapy in a neuroblastoma cell line. *Cancer Res* **61**: 8–13.

Tweddle DA, Pearson AD, Haber M, Norris MD, Xue C, Flemming C *et al.* (2003). The p53 pathway and its inactivation in neuroblastoma. *Cancer Lett* **197**: 93–98.

Wong HK, Fricker M, Wyttenbach A, Villunger A, Michalak EM, Strasser A *et al.* (2005). Mutually exclusive subsets of BH3-only proteins are activated by the p53 and c-Jun N-terminal kinase/c-Jun signaling pathways during cortical neuron apoptosis induced by arsenite. *Mol Cell Biol* **25**: 8732–8747.

Wei MC, Zong WX, Cheng EH, Lindsten T, Panoutsakopoulou V, Ross AJ *et al.* (2001). Proapoptotic BAX and BAK: a requisite gateway to mitochondrial dysfunction and death. *Science* **292**: 727–730.

Wolff A, Technau A, Ihling C, Technau-Ihling K, Erber R, Bosch FX *et al.* (2001). Evidence that wild-type p53 in neuroblastoma cells is in a conformation refractory to integration into the transcriptional complex. *Oncogene* **20**: 1307–1317.

Yakovlev AG, Di Giovanni S, Wang G, Liu W, Stoica B, Faden AI. (2004). BOK and NOXA are essential mediators of p53-dependent apoptosis. *J Biol Chem* **279**: 28367–28374.

■ 特集　小児固形腫瘍の分子生物学（その 3）：最新の知見

Ewing 肉腫ファミリー腫瘍の分子生物学

大喜多　肇*

はじめに

Ewing 肉腫ファミリー腫瘍（Ewing's sarcoma family tumor：ESFT）は，小児や若年成人の骨軟部に好発する腫瘍であり，原発性悪性骨腫瘍のなかでは骨肉腫に次ぐ頻度とされている。本腫瘍群には Ewing 肉腫，peripheral primitive neuroectodermal tumor（PNET）が含まれる。両腫瘍は，元来，異なる腫瘍として報告されてきたが，共通する染色体転座と病理組織学的特徴により，現在では，同一の範疇に入る腫瘍と考えられている。本稿では，ESFT における融合遺伝子の病理学的あるいは臨床的な意義と腫瘍発生における生物学的な意義について概説したい。

Ⅰ．病理組織学的特徴

Ewing 肉腫と PNET では，小型類円形でクロマチンの増量した核と明るい細胞質を有する腫瘍細胞が，繊細な血管性間質を伴ってびまん性に増殖する。Ewing 肉腫はほとんど分化形質を示さない。一方，PNET では Homer-Wright 型の偽ロゼットがしばしば認められ，免疫組織化学的に neuron specific enolase や neurofilament などの神経系のマーカーの発現が認められる。しかしながら，同一の腫瘍内にほとんど分化形質を示さない Ewing 肉腫の組織像を示す部と，神経系の形質を示す PNET の組織像を示す部が混在することもあり，Ewing 肉腫，PNET を明確に区別することは困難なこともある。これらの腫瘍は，免疫組織学的には CD99（MIC2）が，びまん性に膜上に陽性となるのが特徴的である。CD99 は ESFT の感度の高いマーカーであるが，リンパ芽球性リンパ腫をはじめとする他の小円形細胞腫瘍においても陽性となることがあり，鑑別診断上，留意する必要がある。

表　ESFT に認められる染色体転座と融合遺伝子

転座の核型	融合遺伝子	頻度
t(11;22)	*EWS-FLI1*	80%
t(21;22)	*EWS-ERG*	15%
t(7;22)	*EWS-ETV1*	まれ
t(17;22)	*EWS-E1AF*	まれ
t(2;22)	*EWS-FEV*	まれ
t(16;21)	*FUS-ERG*	まれ
t(2;16)	*FUS-FEV*	まれ

Ⅱ．分子遺伝学的特徴

ESFT の約 80%に特徴的な染色体転座 t(11;22) が存在し，転座による融合遺伝子 *EWS/FLI1* が単離された（表）[1,2]。さらに約 15%には t(21;22) に由来する EWS/ERG 遺伝子が存在する。この 2 つの融合遺伝子に加え，頻度は非常に低いが，*EWS/ETV1*, *EWS/E1AF*, *EWS/FEV* といった融合遺伝子が報告されている[3]。これらの融合遺伝子はいずれも 5′側が *EWS* 遺伝子（EWSR1, Ewing sarcoma breakpoint region 1）で，3′側が ETS family に属する転写因子であり，*EWS/ETS* 融合遺伝子とも呼ばれている。*EWS* 遺伝子の産物は，RNA 結合蛋白質と考えられ，類似した構造を有する FUS（fusion in malignant liposarcoma），TAF II 68（TAF15, TAF15 RNA polymerase II，TATA box binding protein（TBP）-associated factor, 68kDa）とともに TET family と呼ばれている。それぞれの融合遺伝子の産物には N 末端側

* 国立成育医療センター研究所発生・分化研究部
〔〒157-8535　東京都世田谷区大蔵 2-10-1〕

の transactivation domain が含まれている。一方，3′側の転写因子には ETS DNA binding domain が in frame で含まれるというのが共通した特徴であり，融合遺伝子は異常な転写因子として作用すると考えられている。さらに，近年，*EWS/ETS* 融合遺伝子に加え，TET ファミリーのメンバーである *FUS* 遺伝子と ETS ファミリーの転写因子による融合遺伝子（*FUS/ERG*, *FUS/FEV*）が報告されている。

Ⅲ. 遺伝子診断

ESFT の病理学的診断は，特徴的な病理組織学的形態と免疫染色（CD99 陽性，他の分化マーカー desmin，TdT などが陰性）によってなされるのが一般的であろう。しかしながら，ごく少量しか腫瘍成分が得られない場合や，免疫染色の染色性が不良の場合など診断に苦慮することが少なくない。このような場合，融合遺伝子の同定が確定診断を下すために重要となる。筋と神経への分化を示す biphenotypic sarcoma で EWS/FLI1 が，desmoplastic round cell tumor で EWS/ERG が検出されたとの報告があること，FUS/ERG が急性骨髄性白血病の一部で同定されるなど，*EWS*（あるいは *FUS*）*/ETS* 融合遺伝子は，ESFT に 100%特異的とはいえないものの，非常に特異性が高いと考えられており，病理組織学的な形態所見と組み合わせて診断を行うことにより，より正確な診断が可能と思われる。一方，頻度は低いものの，融合遺伝子が検出されないが病理学的には ESFT と考えざるを得ない症例も存在する。このような場合は，病理組織学的鑑別診断（リンパ芽球性リンパ腫や低分化型の滑膜肉腫など）を十分考慮したうえで，ESFT の診断を下すべきであろう。

ESFT の場合，EWS と ETS family の転写因子が，さまざまな exon の組み合わせで融合するサブタイプが存在する。このことから，RT-PCR 法で遺伝子診断する場合，融合遺伝子に由来する PCR 産物の長さが症例により一定ではなく，シークエンスによる塩基配列の確認が必要な場合もある。さらに，パラフィン包埋ブロックを用いた RT-PCR の場合，標的とする配列を 100 塩基程度に短くする必要があるため，それぞれのサブタイプに応じた PCR プライマーの設計が必要であり，まれなサブタイプの検出は現実的には困難である。

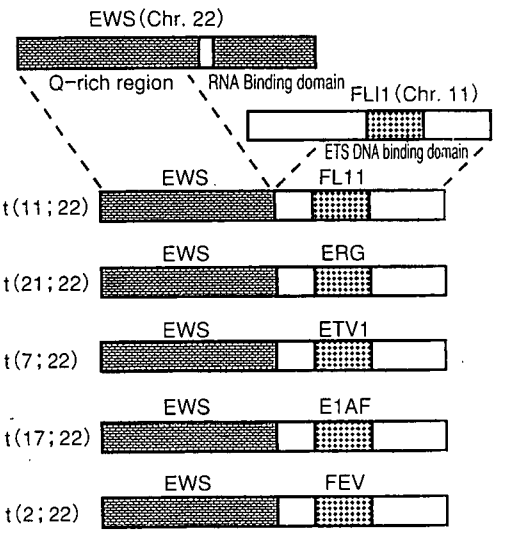

図 ESFT にみられる EWS 関連融合遺伝子の模式図
EWS の N 末端側には Q (glutamine)-rich region があり，FLI1 の C 末端側には ETS DNA binding domain がある。

各融合遺伝子のサブタイプと予後との関連については，差がないという報告もあるが，*EWS/FLI1* の type 1 とそれ以外の融合遺伝子を有する腫瘍では，前者のほうが予後が良いという報告もなされており，今後，さらに検討されるべき課題である[4]。また，骨髄や末梢血における融合遺伝子の検索によって微小残存病変を感度良く検出できると報告されているが，これらの臨床的意義の評価は現時点では定まっていない。

Ⅳ. 融合遺伝子による腫瘍発生機序

EWS/ETS 融合遺伝子は ESFT のほぼすべてに存在すること，*EWS/FLI1* は NIH3T3 をトランスフォームする能力を有することから，*EWS/ETS* は ESFT の腫瘍発生に非常に重要な役割を演じていると考えられている。*EWS/ETS* は，ETS DNA binding domain を有することから異常な転写因子として機能すると考えられており，その標的遺伝子が探索されてきた。これまで同定

された遺伝子のなかには，c-*Myc*（細胞周期やアポトーシスに関与するがん遺伝子）や CCND1 (cyclin D1，細胞周期関連分子)，PDGFC (platelet derived growth factor C, 間葉系細胞に作用する増殖因子)，Nkx2.2 (NK2 homeobox 2，神経細胞の分化にかかわるホメオボックスを有する分子)，NR0B1（オーファン核内受容体)，Id2 (inhibitor of DNA binding 2，bHLH 転写因子に対して抑制性に作用する分子）などが報告されている[5,6]。

また，融合遺伝子は転写を上昇させるばかりでなく，TGFBRII (TGF-βtype 2 receptor）や IGFBP-3 (insulin-like growth factor-binding protein 3）のように融合遺伝子によって発現が抑制される分子も報告されている[7]。前述した分子に加えて，さまざまな培養細胞への融合遺伝子導入実験により，*EWS/ETS* 融合遺伝子の産物はかなり多数の遺伝子の転写を直接的あるいは間接的に制御していると考えられつつあり，ひとつの遺伝子の制御のみで腫瘍発生を説明することはできないようである。今後は，各標的分子が腫瘍発生に果たす役割を明確にするとともに，どの分子が腫瘍の発症，維持に重要であるか解明する必要があるであろう。

さまざまな培養細胞に融合遺伝子を発現させることによって，その腫瘍発生における役割が解析されてきた。マウスの線維芽細胞である NIH3T3 細胞が，*EWS/FLI1* の強制発現によりトランスフォームされ，ESFT の形質の一部が出現することが報告されている。また，*EWS/FLI1* の強制発現により神経芽腫や横紋筋肉腫に ESFT のマーカーが発現するなど，融合遺伝子はトランスフォーム能があるのみならず，細胞の分化形質も制御するものと考えられる。一方，ヒトの線維芽細胞に融合遺伝子を強制発現させてもトランスフォームされず，ESFT 様の形態変化も生じないようである。これらのことからヒトの細胞では融合遺伝子のみではトランスフォームに不十分で他の遺伝子異常なども必要と推測されるとともに，細胞の環境により融合遺伝子が発揮する効果が異なる可能性も考えられる。

一方，RNAi を用いて ESFT 細胞において *EWS/FLI1* をノックダウンすると，ソフトアガー上でのコロニー形成能が失われること，ヌードマウスでの腫瘍形成能が抑制されることが示された[5]。このことは，前述した強制発現の結果とあわせ，*EWS/FLI1* が ESFT にとって必須であることを示している。さらに，*EWS/FLI1* をノックダウンした ESFT 細胞の遺伝子発現プロファイルは，間葉系幹細胞に近づくこと，*EWS/FLI1* をノックダウンした ESFT 細胞は，脂肪や骨への分化能を示し，間葉系幹細胞様の性質が出現することが示された[8]。さらに，マウスの骨髄由来間葉系前駆細胞に *EWS/FLI1* を強制発現させると，ESFT 類似の腫瘍を形成しうることも報告された[9]。ESFT の発生母地は，未熟な間葉系細胞，神経堤細胞などの説が唱えられているが，これらの結果からは，間葉系幹細胞あるいはそれに近い細胞が ESFT の起始細胞であることが示唆される。今後，ヒト間葉系幹細胞/前駆細胞における *EWS/ETS* の機能が解明されることが期待される。

おわりに

融合遺伝子の発見以来，ESFT の疾患概念が整理されるとともに，その腫瘍発生における機能が盛んに研究されてきた。*EWS/FLI1* がある種の細胞に対してトランスフォーム能を有すること，ESFT 様の形質を与えることから，ESFT 発症において融合遺伝子が重要な役割を演じていると信じられているが，その作用機構にはいまだに解明すべき点が残されている。今後は融合遺伝子による ESFT 発症モデルの作製や，ESFT の起始細胞の同定，その起始細胞における *EWS/ETS* の機能解析が期待される。

文　献

1) Delattre O, Zucman J, Plougastel B, et al : Gene fusion with an ETS DNA-binding domain caused by chromosome translocation in human tumours. Nature. 359 (6391) : 162-165, 1992
2) May WA, Gishizky ML, Lessnick SL : Ewing sarcoma 11 ; 22 translocation produces a chimeric transcription factor that requires the DNA-bind-

ing domain encoded by FLI I for transformation. Proc Natl Acad Sci 90 : 5752-5756, 1993
3) Kovar H : Ewing's sarcoma and peripheral primitive neuroectodermal tumor s after their genetic union. Cur Opin in Oncol 10 : 334-342, 1998
4) de Alava E, Kawai A, Healey JH, et al : EWS-FLI1 fusion transcript structure is an independent determinant of prognosis in Ewing's sarcoma. J Clin Oncol1 16 (4) : 1248-1255, 1998
5) Smith R, Owen LA, Trem DJ, et al : Expression profiling of EWS/FLI identifies NKX2.2 as a critical target gene in Ewing's sarcoma. Cancer Cell 9 : 405-416, 2006
6) Fukuma M, Okita H, J Hata, et al : Upregulation of Id2, an oncogenic helix-loop-helix protein, is mediated by the chimeric EWS/ets protein in Ewing sarcoma. Oncogene 22 (1) : 1-9, 2003
7) Hahm KB, Cho K, Lee C, et al : Repression of the gene encoding the TGF-beta type II receptor is a major target of the EWS-FLI1 oncoprotein. Nat Genet 23 (2) : 222-227, 1999
8) Triode F, Laud-Duval K, Prieur A, et al : Mesenchymal Stem Cell Features of Ewing Tumors. Cancer Cell 11 : 421-429, 2007
9) Riggi N, Cironi L, Provero P, et al : Development of Ewing's sarcoma from primary bone marrow derived mesenchymal progenitor cells. Cancer Res 65 11459-11468, 2005

Molecular Biology of the Ewing's Sarcoma Family of Tumors

HAJIME OKITA

Department of Developmental Biology, National Research Institute for Child Health and Development

Key words : Fusion gene, Ewing's sarcoma, Transcription factor, Molecular biology.
Jpn. J. Pediatr. Surg., 39(11) ; 1344～1347, 2007.

The Ewing's sarcoma family of tumors (ESFT) are bone and soft tissue sarcomas that occur in children and young adults. Specific chromosomal translocations found in ESFT cause EWS to fuse to a subset of ets transcription factor genes (ETS), generating chimeric EWS/ETS proteins. These proteins are believed to act as an aberrant transcriptional regulator and play a crucial role in the development of ESFT. The mechanisms responsible for the EWS/ETS-mediated tumorigenesis are well studied but remain uncertain. This review highlights recent advances in the molecular biology of ESFT.

* * *

GENES, CHROMOSOMES & CANCER 46:929–935 (2007)

Duplication of the Paternal *IGF2* Allele in Trisomy 11 and Elevated Expression Levels of *IGF2* mRNA in Congenital Mesoblastic Nephroma of the Cellular or Mixed Type

Naoki Watanabe,[1,2] Masayuki Haruta,[1] Hidenobu Soejima,[3] Daisuke Fukushi,[1] Kinji Yokomori,[4] Hisaya Nakadate,[4] Hajime Okita,[4] Jun-ich Hata,[4] Masahiro Fukuzawa,[4] and Yasuhiko Kaneko[1,4]*

[1]Department of Cancer Diagnosis, Research Institute for Clinical Oncology, Saitama Cancer Center, Ina, Saitama, Japan
[2]Department of Pediatrics, Juntendo University, Nerima Hospital, Nerima-Ku, Tokyo, Japan
[3]Department of Biomolecular Sciences, Faculty of Medicine, Saga University, Saga, Japan
[4]Japan Wilms Tumor Group Study, Itabashi-Ku, Tokyo, Japan

In a metaphase comparative genomic hybridization and fluorescence in situ hybridization study of 13 congenital mesoblastic nephroma (CMN) tumors, trisomy 11 was found in seven cellular or mixed type tumors, disomy 11 with other chromosome changes in two cellular type tumors, and no chromosome changes in four classical type tumors. Reverse-transcription (RT)-PCR analysis detected the *ETV6-NTRK3* fusion transcript in all eight cellular or mixed type tumors examined, but not in four classical type tumors. All seven tumors with trisomy 11 showed duplication of the paternal *IGF2* allele, and six cellular or classical type tumors with disomy 11 showed one paternal and one maternal allele of *IGF2*, analyzing the methylation status of the sixth CTCF site of the *H19*-differentially methylated region. Allelic expression study using the *ApaI/AvaII* polymorphism site at exon 9 of *IGF2* showed retention of imprinting in all seven tumors examined. Quantitative real-time RT-PCR analysis showed higher expression levels of *IGF2* mRNA in three of three cellular type tumors with trisomy 11, in one cellular type tumor with disomy 11, and in three of four classical tumors than in fetal kidneys or normal kidney tissues. Thus, duplicated paternal *IGF2* resulted in elevated *IGF2* mRNA levels, and may provide CMN or its precursor cells with a proliferative advantage. The mechanism explaining that some cellular or classical type tumors with disomy 11 also showed elevated *IGF2* mRNA levels remains unresolved. *IGF2* clearly plays an important role in the tumorigenic process of CMN, although it is difficult to assess its exact role.

INTRODUCTION

Congenital mesoblastic nephroma (CMN) is a spindle cell tumor of the kidney occurring in newborns or young infants; it is subclassified into cellular, mixed, and classical types. Cellular type CMN shows increased cellularity with high mitotic activity, and classical type CMN displays moderate cellular proliferation of fibroblastic cells, whereas mixed type CMN shows admixtures of the two patterns (Schofield et al., 1993; Knezevich et al., 1998a). Molecular and cytogenetic studies of cellular or mixed type CMN have demonstrated that they are characterized by an *ETV6-NTRK3* fusion gene and that trisomy 11 is frequent, while the characteristics of classical type CMN remain obscure (Schofield et al., 1993; Knezevich et al., 1998a; Rubin et al., 1998; Watanabe et al., 2002).

Active growth-promoting genes or mutated oncogenes are expected to reside on the duplicated chromosome 11 in CMN. A prime candidate is the *IGF2* gene, because the overexpression of *IGF2* mRNA was reported in CMN, and one study reported that an intact IGF signaling axis is essential for in vitro *ETV6-NTRK3*-mediated transformation (Sharifah et al., 1995; Morrison et al., 2002). *IGF2* is subjected to imprinting and is expressed from the paternal allele. *IGF2* is located in 11p15.5 and encodes a fetal polypeptide growth factor.

Loss of heterozygosity (LOH) of *IGF2* resulting in the loss of the maternal allele and duplication of the paternal allele or loss of imprinting (LOI) of *IGF2* is present in a majority of Wilms tumors, another embryonal kidney tumor (Yuan et al.,

Supported by: Ministry of Education, Science, Sports and Culture of Japan; Grant number: 18790745; Ministry of Health, Labor and Welfare, Japan for Third Term Comprehensive Control Research for Cancer.

*Correspondence to: Yasuhiko Kaneko, Research Institute for Clinical Oncology, Saitama Cancer Center, 818 Komuro, Ina, Saitama 362-0806, Japan. E-mail: kaneko@cancer-c.pref.saitama.jp

Received 12 June 2007; Accepted 29 June 2007

DOI 10.1002/gcc.20481

Published online 18 July 2007 in Wiley InterScience (www.interscience.wiley.com).

TABLE 1. Clinical and Molecular-Genetic Findings in 13 Congenital Mesoblastic Nephroma Tumors

Patient	Age/sex	*ETV6/NTRK3*	mCGH findings	No. of chr. 11 by FISH	% methylated CTCF6 allele	*IGF2* status by RT-PCR	Relative quantity of *IGF2* mRNA
Cellular or mixed type (n = 9)							
1	5d/F	Positive	enh(11)	3	66.1	ROI	6.2
2	15d/F	Positive	enh(11)	Not done	76.6	ROI	2.2
3	24d/M	Positive	enh(11)	Not done	62.9	ROI	Not done
4	1m/M	Positive	enh(8,11)	3	65.8	Not informative	2.4
5[a]	1m/M	Positive	enh(11)	3	64.2	ROI	Not done
6	1m/M	Positive	enh(11)	3/4	66.9	ROI	Not done
7	5m/F	Not done	enh(11)	Not done	87.1	Not done	Not done
8	7m/F	Positive	enh(12p13-q24), dim(15q23-qter)	2	51.4	Not informative	2.6
9[b]	13m/F	Positive	enh(17q),dim(X)	2	54.3	Not informative	0.1
Classical type (n = 4)							
10	7d/M	Negative	No changes	Not done	50.8	Not informative	2.9
11	23d/M	Negative	No changes	2	52.3	ROI	6.3
12	4m/M	Negative	No changes	2	51.1	Not informative	4.6
13	2m/F	Negative	No changes	Not done	49.3	ROI	0.5
Human fetal kidney total RNA							1.5
Normal kidney tissues (N1, 6m; N2, 21m, N3, 21m)							0.3, 0.1, 0.1

mCGH, metaphase CGH; chr.11, chromosome 11; d, days; m, months; F, female; M, male; enh, enhanced; ROI, retention of imprinting.
[a]This tumor was classified as the mixed type, and the other eight as the cellular type.
[b]A CMN cell line established from a tumor resected from the patient was studied.

2005; Watanabe et al., 2006). The status of *IGF2* in previous studies of CMN tumors is controversial. Becroft et al. (1995) found LOI of *IGF2* in one tumor, whereas Watanabe et al. (2002) found retention of imprinting (ROI) of *IGF2* in 2 tumors. In addition, Speleman et al. (1998) reported LOH at 11p15 in one tumor in their study. Another study mentioned, without providing data, that an extra copy of chromosome 11 was paternally derived in two CMN and congenital fibrosarcoma primary tumors (Morrison et al., 2002).

In the present study, we performed metaphase comparative genomic hybridization (mCGH) and examined the LOI or LOH status of *IGF2*, the methylation status of CTCF6 at *H19*-differentially methylated region (DMR) that represents the parental origin of the *IGF2* allele (Takai et al., 2001), and the quantity of *IGF2* mRNA in the three types of CMN. Our results showed a paternal origin of the duplicated chromosome 11 and an elevated expression level of *IGF2* mRNA in all cellular type tumors with trisomy 11 and in some cellular or classical type tumors with disomy 11.

MATERIALS AND METHODS

Patients and Samples

Tumor samples were obtained from 13 Japanese infants with CMN ranging in age from newborn to 13 months (Table 1). Some data from 5 of the 13 patients were previously reported (Watanabe et al., 2002). Eight tumors were classified as the cellular type, one as the mixed type (No. 5), and the other four as the classical type by pathologists at each institution or the Japan Wilms tumor study group pathology panel according to the classification proposed by the Japanese Pathological Society (1988). One tumor tissue (No. 9) was obtained from a cell line (MN-JRC-24) established from a CMN tumor by one (KY) of the authors. The patient was a 13-month-old girl who presented with a right abdominal tumor of stage 2, according to the NWTS staging system (D'Angio et al., 1989). She received the NWTS-3 protocol regimen K after surgery, but developed metastasis to the thoracic vertebrae, the ilium and the right humerus, and died of the disease 15 months after the start of surgery and chemotherapy. The tumor sample obtained at the time of surgery was used to establish the cell line. All but one (No. 9) patient showed no evidence of the disease at the last follow-up.

Metaphase Comparative Genomic Hybridization and Fluorescence In Situ Hybridization Analysis

A metaphase comparative genomic hybridization (mCGH) analysis was performed on all 13 tumors to evaluate chromosome gains and losses as described (Kumon et al., 2001). Interphase fluorescence in situ hybridization (FISH) was performed in eight tumors using probes, including a YAC probe (964c10) covering the *ETV6* locus on 12p13, a BAC probe (RP11-285I-14) covering exons 13–18 of the *NTRK3* gene on 15q26 (GenBank accession number: AC011966), and a BAC probe (ATCC

65438) covering the centromeric region of chromosome 11.

RT-PCR of *ETV6-NTRK3* mRNA and Quantitative Real-time RT-PCR of *IGF2* mRNA

Frozen tumor tissues were extracted from 12 tumors, first-strand cDNA was synthesized, and PCR was performed with primers: ETV6/541 (5′-CCTCCCACCATTGAACTGTTGCACC-3′) located in exon 5 and NTRK3-ex14r (5′-CGCACACTCCATAGAACT-3′) located in exon 14. RT-PCR products were purified and directly sequenced on a sequencer (Applied Biosystems, Foster City, CA).

Quantitative real-time RT-PCR was performed to evaluate *IGF2* mRNA levels in nine tumors, human fetal kidney total RNA pooled from 34 spontaneously aborted fetuses (Clontech, Ohtsu, Japan), and three normal kidney tissues adjacent to Wilms tumors using LightCycler TaqMan Master on the LightCycler Carousel-Based System (Roche Diagnostics, Alameda, CA). The three patients whose normal kidney tissues were used were six months, 21 months, and 21 months of age. As described previously (Ravenel et al., 2001) with slight modifications, we used 5′-CCCCTCCGACCGTGCT-3′ (forward primer), 5′-TCATATTGGAAGAACTTGCCCA-3′ (reverse primer), and FAM-5′-CCGGACAACTTCCCCAGATACCC-3′-BHQ-1 as primers and a TaqMan probe. Each sample was analyzed in triplicate with *GAPDH* as the inner control, and the mean value of *IGF2* mRNA was calculated.

Allelic Expression Analysis of *IGF2* and LOH Analysis of the 11p15 Region

The *Apa*I/*Ava*II polymorphism site in exon 9 of *IGF2* was used to evaluate the allelic status and expression of *IGF2*. PCR with genomic DNA from tumor tissues and the identification of heterozygous specimens after *Apa*I digestion were performed as described previously (Watanabe et al., 2002). LOH analysis of the 11p15 region was performed using microsatellite markers as described previously (Watanabe et al., 2006).

Combined Bisulfite Restriction Assay of the CTCF6 Site in *H19*-DMR

To clarify the parental origin of *IGF2* alleles on duplicated chromosome 11, we performed combined bisulfite restriction assay (COBRA) of CTCF6 in *H19*-DMR (Xiong and Laird, 1997; Takai et al., 2001; Satoh et al., 2006). Genomic

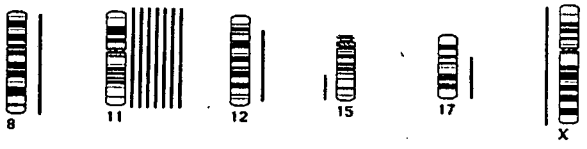

Figure 1. Summary of CGH findings obtained from nine patients with congenital mesoblastic nephroma of the cellular or mixed type. Gains are shown on the right side of the chromosome ideogram and losses on the left side. Lines represent regions of chromosomal gains and losses.

DNA from 13 tumor samples was treated with sodium bisulfite and subjected to PCR using primer sets: 5′-GAGTTYGGGGGTTTTTGTATAGT-3′ and 5′-TAAATAATACCCRACCTAAAATCTAA-3′ designed to amplify the region including CTCF6. Normal lymphocyte DNA treated with *Sss*I methyltransferase (New England Biolabs, Ipswich, MA) was used as a control for methylated templates, and lymphocyte DNA without *Sss*I treatment as a control for a methylated and unmethylated template ratio of 1:1. *Mlu*I recognizes the methylated but not the unmethylated acgcgt sequence located in the vicinity of the sixth CTCF sequence of cgcgcggcg; the methylation status of the former sequence closely reflects that of the latter sequence. PCR products digested with *Mlu*I were run on 2% NuScieve agarose gel (FMC Bioproducts, Rockland, ME) and visualized after ethidium bromide staining. The intensity of methylated and unmethylated bands was examined using a fluoro-image analyzer, FLA-3000G (Fujifilm, Tokyo). The size of the unmethylated band was 279 bp, and there were two methylated bands; 197 bp and 82 bp. Only the larger band was evaluated because the smaller one was too faint in intensity to be evaluated in all samples. The experiments were performed three times, and the mean value of the DNA methylation percentages was calculated. The hot-stop COBRA method was used to confirm the data detected by the standard COBRA method (Uejima et al., 2000).

RESULTS

An mCGH study showed enhanced whole chromosome 11, indicating trisomy or tetrasomy 11 in seven of nine cellular or mixed type tumors; one of these seven cases also showed enhanced whole chromosome 8. The remaining two cellular type tumors showed a normal intensity of chromosome 11, indicating disomy 11; one (No. 8) had enhanced 12p13-12q23 and dim 15q23-15qter regions, and the other (No. 9) had enhanced 17q and dim whole chromosome X. The mCGH pattern is summarized in Figure 1. Subsequent cyto-

genetic and FISH study of the latter tumor (No. 9) showed the karyotype 45,X,-X,t(12;15)(p13;q26), der(14)t(14;17)(q32;q12). Four classical type tumors had normal intensity in all chromosomes and two (Nos. 11 and 12) of the four showed a normal karyotype (Table 1). The results of FISH analysis of eight tumors using the chromosome 11 centromere probe were consistent with those of mCGH analysis (Table 1).

ETV6-NTRK3 fusion mRNA was detected in all eight cellular or mixed type tumors examined, but not in all four classical type tumors (Table 1). All eight tumors showed the same breakpoints at *ETV6* exon 5 and *NTRK3* exon 13, as reported previously (Knezevich et al., 1998b). Interphase FISH analysis showed the *ETV6-NTRK3* fusion signal in all six cellular or mixed type tumors (Nos. 1, 4–6, 8, and 9) examined, but not in two classical type tumors examined (Nos. 11 and 12). The results of the FISH study were consistent with the RT-PCR study.

Twelve tumor samples were available for the allelic expression study of *IGF2*, and all seven with the heterozygous *Apa*I site showed the monoallelic expression of *IGF2*, indicating the retention of imprinting (ROI) of *IGF2* (Table 1 and Fig. 2). These seven tumor samples retained heterozygosity at the *IGF2* locus. Of the remaining five tumors with the homozygous *Apa*I/*Ava*II site, four showed heterozygosity at least in one of three 11p15.5 loci; i.e. *D11S922*, *TH*, or *D11S932*, and the other tumor (No. 9) showed homozygosity at all three loci: the presence or absence of LOH was not determined because normal tissue was not available. One tumor (No. 7) with no RNA available showed heterozygosity at the *TH* and *D11S922* loci. These findings indicate that all but one tumor retained heterozygosity at the 11p15 loci.

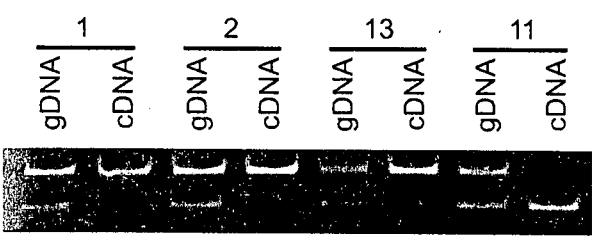

Figure 2. Examples of allelic expression analysis using the *Apa*I polymorphism site at exon 9 of *IGF2*. Electrophoretic pattern of genomic PCR products after *Apa*I digestion shows heterozygosity in tumors 1, 2, 13, and 11, and RT-PCR products after digestion show monoallelic *IGF2* expression, indicating the retention of imprinting in all four samples.

COBRA showed that the mean methylation percentage of *Sss*I-untreated lymphocytes was 49.0%. Seven tumors with trisomy 11 showed a mean methylation percentage ranging from 62.9% to 87.1%, indicating a paternal origin of the duplicated chromosome 11. Six tumors with disomy 11 showed a methylation percentage ranging from 49.3 to 54.3%, indicating ROI of *IFG2*, but not LOH or LOI of *IGF2*. The results are summarized in Table 1 and Figure 3. The results of COBRA analysis using the hot-stop method for 13 tumor and two peripheral blood samples were consistent with those of standard COBRA analysis (data not shown).

Quantitative real-time RT-PCR analysis showed almost no expression of *IGF2* mRNA in two normal kidney tissues obtained from 21-month-old patients (N2 and N3) and in one cultured sample established from a cellular type tumor with disomy 11. Small amounts of *IGF2* mRNA were found in normal kidney tissue obtained from a 6-month-old patient (N1) and in a classical type tumor (No. 13), and moderate amounts were found in human fetal kidney total RNA. All three cellular type tumors with trisomy 11, one cellular type tumor with disomy 11, and three classical type tumors showed higher expression levels of *IGF2* mRNA than three normal kidney tissues or human fetal total RNA (Table 1 and Fig. 4).

DISCUSSION

Histological studies have suggested that cellular and classical type CMN tumors are related to congenital fibrosarcoma (CFS) and infantile fibromatosis (IFS), respectively (Schofield et al., 1993, 1994; Knezevich et al., 1998a). Moreover, molecular

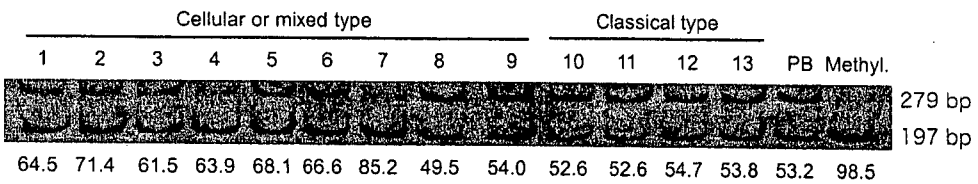

Figure 3. Examples of the methylation status of CTCF6 analyzed by a combined bisulfite restriction assay (COBRA). Bisulfate-modified PCR products were digested with *Mlu*I. Numbers above lanes indicate the tumor number. Upper 279 bp and lower 197 bp bands show unmethylated and methylated DNA fragments containing CTCF6, respectively. PB, lymphocyte DNA without *Sss*I treatment; Methyl, methylated lymphocyte DNA with *Sss*I treatment. The percentage of methylated DNA calculated from the bands above is shown below each lane. The mean value of the DNA methylation percentages calculated from three COBRA experiments is shown in Table 1.